25th ABCM International Congress of Mechanical Engineering
October 20-25, 2019, Uberlândia, MG, Brazil

COB-2019-1233
Macrostructure, Microstructure and Microhardness of an AISI SAE 1020 Steel Welded Joint by GMAW Active Gas Process

Gianfranco de Mello Stieven
Daniele dos Reis Soares
Taiane Pereira Pantoja
Federal University of Pará, Augusto Corrêa St., 1 - Guamá, Belém - PA, 66075-110
gianfrancostieven@yahoo.com.br
dani_ddrs@yahoo.com.br
taianepereira23@gmail.com

Edilma Pereira Oliveira
Federal University of South and Southest of Pará, Block Four (Fl.17), New Marabá, Marabá - PA, 68505080
edilma@unifesspa.edu.br

Erb Ferreira Lins
Jorge Teófilo de Barros Lopes
Federal University of Pará, Augusto Corrêa St., 1 - Guamá, Belém - PA, 66075-110
erb@ufpa.br
teofilo@ufpa.br

Abstract. *The Gas Metal Arc Welding (GMAW) process is commonly employed in the manufacture and maintenance of metal parts and equipment. However, this process has greater sensitivity to the variation of the electric parameters of welding arc operation, which influence the quality of the weld, and still needs a strict adjustment of parameters to obtain a certain set of characteristics for the weld bead. Therefore, papers are developed with the purpose of promoting improvements in the GMAW process and the quality of welded joint. Thus, this work aims to characterize an AISI SAE 1020 steel-welded joint with electrode ER80S-G by the MAG welding process, analyzing the macrostructure, microstructure and microhardness, given a fixed set of welding parameters, such as voltage, nozzle-to-work distance, feed rate, welding speed etc. Due to the welding parameters used during the process, the macrostructure revealed a little discontinuity in the part caused by lack of penetration. The microhardness, on its turn, combined with the microstructure analysis, revealed that the central region of the root of weld, and the top of the weld bead, presented higher microhardness, in the order of 250 and 300 HV, respectively.*

Keywords: *MAG welding, AISI SAE 1020 steel, macrostructure, microstructure, microhardness*

1. INTRODUCTION

According to Sumesh *et al.* (2018), GMAW is a widely used industrial process in which an electric arc is generated and maintained between the electrode wire and the welding sample. This process can be called MAG (Metal Active Gas) or MIG (Metal Inert Gas), depending on the nature of the gas. The MAG process was introduced in the early 1930s in steel parts, which is suitable for welding low carbon steels and low alloy steels (Wainer *et al.*, 2004). This process is commonly used in the manufacture and maintenance of metal equipment and parts, in the recovery of worn parts and in the coating of metal surfaces with special materials (Modenesi *et al.*, 2005). Due to its versatility and high productivity, GMAW welding has been growing worldwide in recent years, due to the tendency to replace manual processes with semiautomatic and mechanized ones. However, the MIG/MAG process has greater sensitivity to the variation of the electric parameters of welding arc operation, which influence the quality of the weld, and still needs a strict adjustment of parameters to obtain a certain set of characteristics for the cord.

Thus, recent studies were developed with the purpose of proposing improvements in the GMAW process, such as: a study of the viability of pulsed ultrasound to control the GMAW process and solder appearance (Chen *et al.* (2018)); the evaluation of the efficiency of wire cleaning and lubrication (Moyses *et al.* (2018)); the effect of the welding parameters on the evaluation of the fusion efficiency (Hackenhaar *et al.* (2018)); and the comparison between the different versions of modern variants of the MIG/MAG process for the root pass in orbital welding (Sartori *et al.* (2017)); and investigating

the effect of multipass welding speed and welding current on the mechanical properties of a AISI SAE 1020 steel in the GMAW process (Bhatti *et al.* (2017)). Therefore, the aim of this paper is to characterize a welded joint of AISI SAE 1020 steel with electrode ER80S-G by the MAG welding process analyzing the following steps: macrostructure, microstructure and microhardness.

2. MATERIALS AND METHODS

The MAG welding process was performed on two AISI SAE 1020 steel plates, each of 10 cm length, V-groove with a 45° angle and a 3 mm nose, to facilitate the execution of the root pass and prevent the part from being poured because it has a minimum thickness. A gas protection composed of Argon (Ar) and 25% of Carbon Dioxide (CO_2) with constant flow of 15 L/min was used. The electrode operated was the ER-80SG, with feed rate and welding velocity of, respectively, 3 m/min and 40 cm/min, 23 V voltage and 15 mm of nozzle-to-work distance. In total, seven passes were made to completely fill the bevel. The specimen was cut in the central region, and in two adjacent symmetrical positions relative to the central cut, in order to allow macrostructural, microstructural and microhardness analysis. To reveal the macrostructure and microstructures resulting from the welding process, the Nital reagent 2% (2 ml of HNO3 in 98 ml of ethyl alcohol) was used, immersed for 4 s. The developed microstructures were visualized through an optical microscope in increments of 50, 500 and 1000 times, while the macrostructures through a stereoscope with an increase of 0.69 time. For the Vickers microhardness analysis, three regions were analysed, as exposed on Fig. 1: the root of weld, the top of weld and the vertical region. A Shimadzu Hmv-M microdurometer, load of 2.942 N and 15 s of indentation time with 0.5 mm pitch was applied in all the regions. The indentation parameters were adjusted according to the work of (Oliveira, 2013). To fill the joint, seven passes were required. The chemical composition of the weld and electrode can be found in Tab. 1.

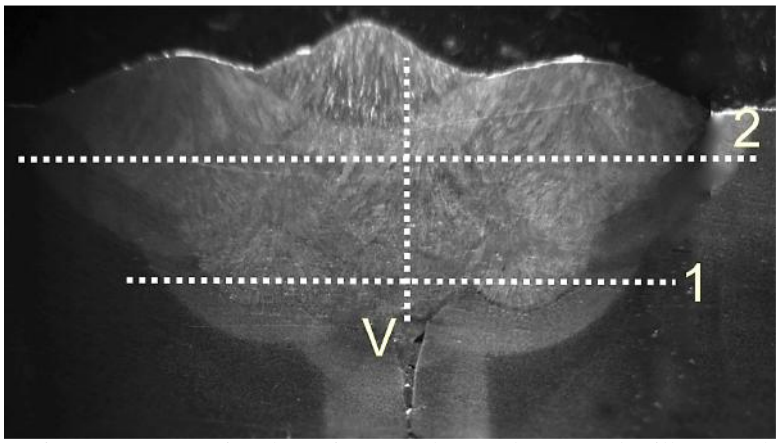

Figure 1: Indented regions in two cross-sectional specimens. The numbers 1 and 2 illustrate the indented region of the root and top respectively, while the letter V is the vertical region of the weld bead.

Table 1: Chemical composition of the base and weld metal.

Chemical Element	AISI SAE 1020	Electrode ER80S-G
Fe	Balance	Balance
C	0.17 - 0.23 %	0.08 %
Mn	0.3 - 0.6 %	1.1 %
P	$\leq$ 0.05 %	-
Si	-	0.6 %
Cr	-	0.4 %
Cu	-	0.5 %

3. RESULTS AND DISCUSSIONS

3.1 Visual Analysis

After defining the welding parameters and performing the process it was found that the welding energy was not adequate for full joint penetration, and it was possible to verify a region without filler metal, as illustrated in Fig. 2. Therefore, it can be consider that the problem of lack of power can be solved by increasing the feed speed, reducing the

welding speed, reducing the nose of the joint, increasing the root opening, etc., or by adjusting more than one variable to in order to optimize the process. Reverse welding, that is, performing a welding pass on the back of the joint to deposit metal in the non-material region could meet the need for penetration, however such a procedure was waived for operational reasons.

Figure 2: Transverse macrostructure of the welded joint.

After the completion of each welding step, a few small islands of silicon can be seen on the surface of the bead, which were easily removed with the help of the mincing hammer. At the end of all passes, there is a weld bead with good surface appearance and homogeneity, without macroscopic cracks, only lack of reinforcement in one of the margins and few splashes. In the penetrating liquid test, porosity concentration can be verified in the region between the passages and the edges of the end passes on the upper face of the weld metal from hot droplets that, when they come into contact with the surface, adhere to it. Despite these problems, the surface of the welded joint has passed the penetrating liquid test because it has no micro cracks.

3.2 Macrostructure

The macrostructure resulting from the welding process can be analyzed from Fig. 3, where it shows the transverse region of the welded joint and the three well defined regions of the weld bead, being the melt pool (or fused zone), the zone thermally affected (or zone affected by heat) and base metal.

It is possible to understand that the majority growth of the grains is driven by the extraction of heat, which characterizes a columnar growth. Given the directional growth, it is observed from the literature that the main phenomenon responsible for dendritic growth in welding processes is the epitaxial and competitive growth of growing grains (Wainer *et al.* (2004)). With the help of Fig. 3, it is verified that in the two studied specimens, emphatically in the upper left corner, that the grains grow due to the grains already existing in the base metal. Figure 4-A and B show the epitaxial growth of the fused zone and Fig. 5-A and B illustrate the competition of columnar grains during growth, which are interrupted by the faster growth of the adjacent grain.

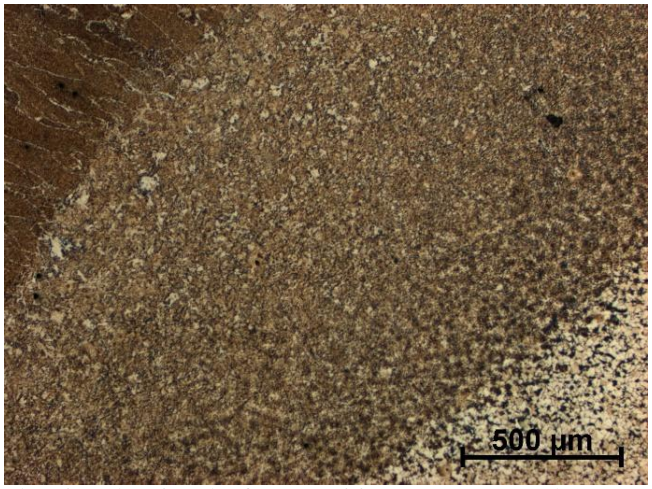

Figure 3: Weld bead region showing the four transition areas commonly reported in the literature.

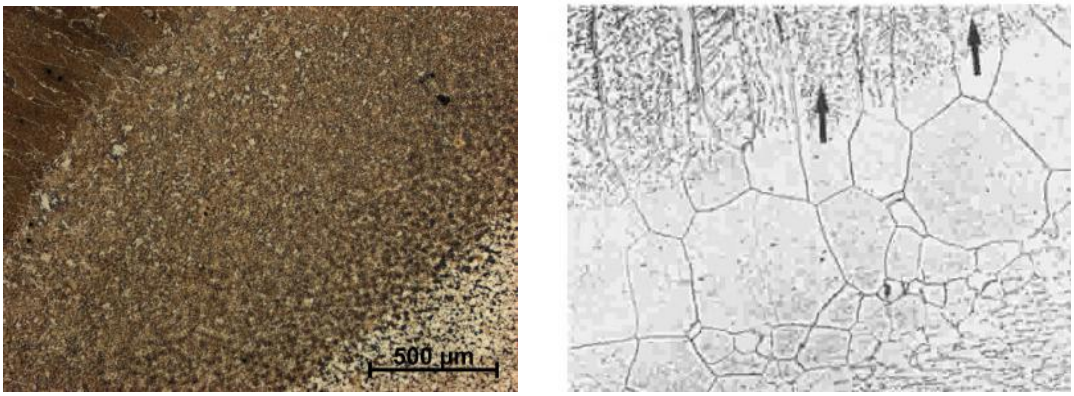

(a) (b)

Figure 4: Grain growth in welding: (a) Epitaxial from base metal and (b) epitaxial illustrated by literature (Easterling (2013)).

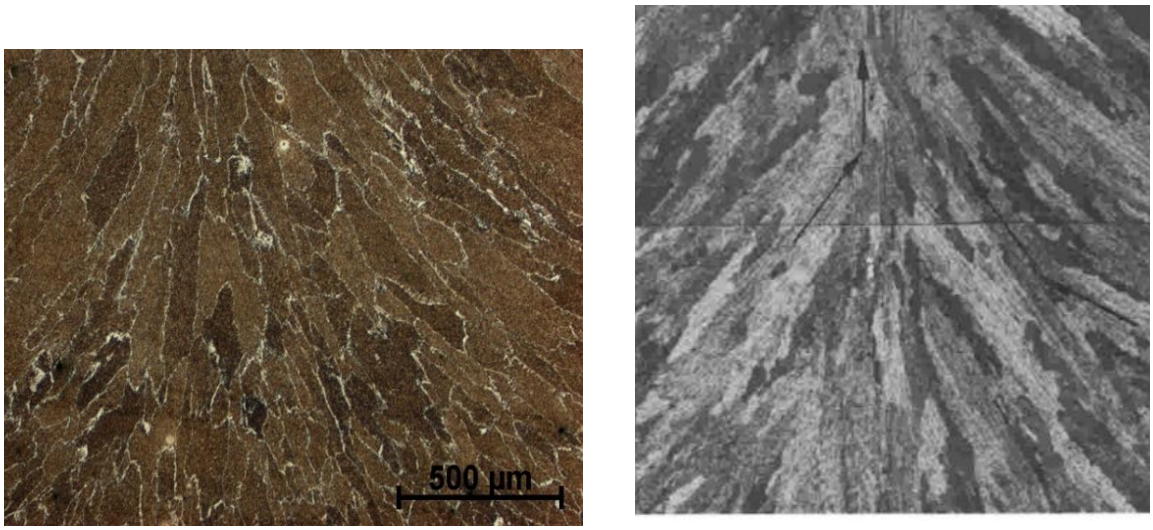

(a) (b)

Figure 5: (a) Competitive growth of heat-driven grains and (b) Competitive growth illustrated in video (Easterling (2013)).

3.3 Microstructure

Because it has several continuous cooling curves, the microstructure of the heat affected zone (HAZ) of a steel can have several regions (Wainer *et al.* (2004)). Therefore, the microstructure of the studied specimen was divided into possible regions presented in the literature, so the results obtained from the micrograph of the pieces, after the welding process in question, can be seen in Fig. 6.

The analysis of the micrographs will be done only by the comparative method between the results obtained in the laboratory and the literature. However, in order to have a larger backing and a reliable foundation, the most coherent would be to have more data from the experiment, such as the thermal cycle of the experiment. process and the deeper identification of the phases present in the material using Scanning Electron Microscopy (SEM). Thus, from the comparative analysis, some structures can be identified by visual similarity, as shown in Fig. 7, which possibly presents martensitic structure, due to its morphology of ferritic slats and retained austenite.

From the microstructure of the region present in the fused zone located at the top of the piece it can be inferred that there is the presence of Widmanstätten ferrite, due to the similarity to the structure with needles starting from the grain boundary. Figure 8 shows the morphology cited above compared to the literature.

Figure 9 shows the formation of possible carbides present in the darker points, it is important to point out that it is only a speculation of such morphology, because for the identification of the microconstituents it is necessary to have a more careful assay for the analysis of such structures, while the Fig. 10 shows the microstructure of the base metal, in which equiaxial ferrite and fine perlite colonies are observed.

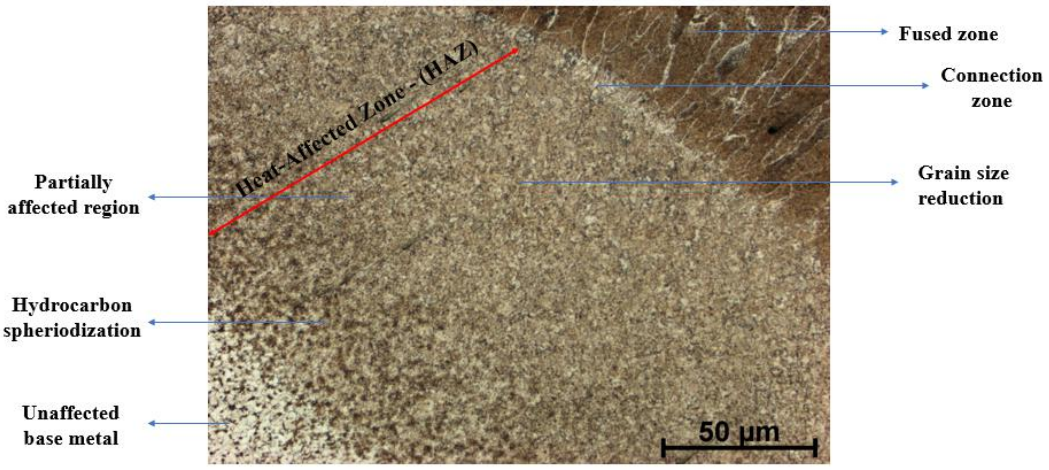

Figure 6: HAZ microstructure with 50 X magnification.

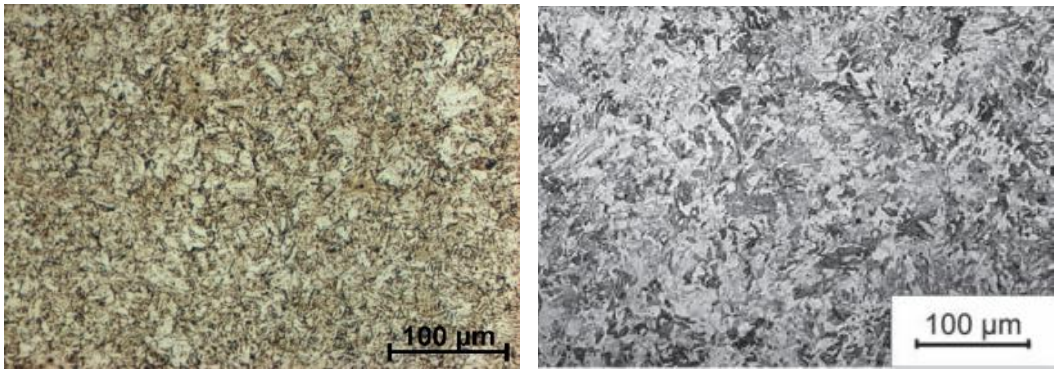

(a) (b)

Figure 7: (a) Microstructure corresponding to the grain refining region, 200X magnification and (b) a martensitic microstructure of high alloy AISM steel (12.01% Cr, 6.4% Ni, 2.42% Mo, 0.47% Mn, 0.17% Si, 0.10% Ti, 0.01% C - weight percent) (Della Rovere *et al.* (2014)).

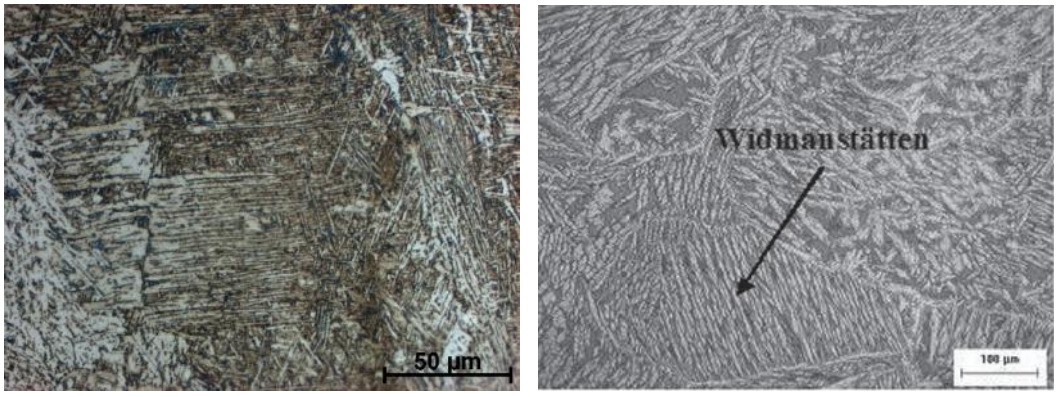

(a) (b)

Figure 8: Microstructure corresponding to the region of the fused zone at the top of the part (a) 500X magnification and (b) Slatted microstructure of the weld metal, HNO_3 attack, 200X magnification (Nunes *et al.* (2012)).

3.4 Microhardness

The data collected from the Vickers microhardness test can be seen from Fig. 11 in which we can see the indentations of point 1 on the left and the point 2 on the right. It can be seen from the graphs in Fig. 11 that the microhardness increases and becomes maximum in a position equivalent to the center of the melt pool. The hypothesis that the region

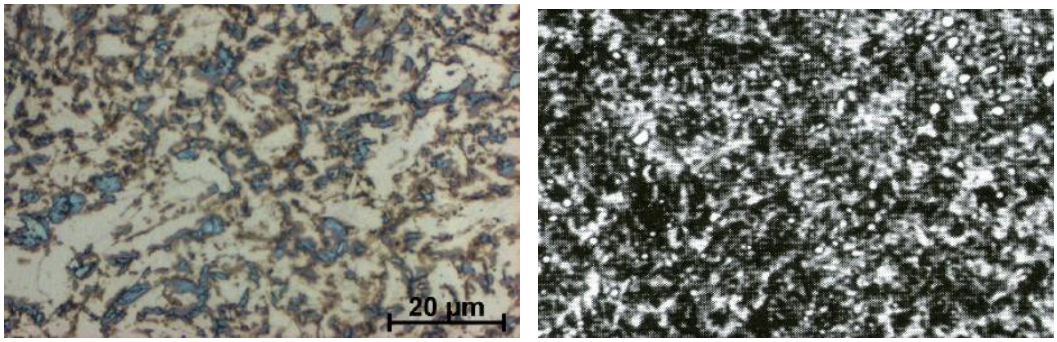

(a) (b)

Figure 9: Microstructure corresponding to partial transform region (a) 500X magnification and (b) O_2 steel showing spheroidized carbides in martensitic matrix (Lyman (1972)).

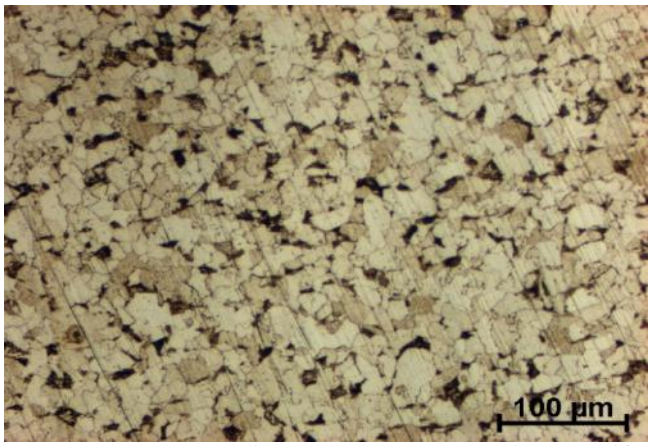

Figure 10: Microstructure corresponding to the base metal region magnification of 200X.

with the highest degree of hardness is the one with the lowest dissolution can be raised, considering that the filler material has higher microhardness compared to the base metal. In the same line of reasoning is presented to Fig. 12, where it can be seen that the fact commented above is ratified. It is reasonable to justify greater hardness in the central region of the joint by the theoretical thermal cycle that the region passes through, which makes available to the volume tetragonal microstructures that distort the crystal lattice, resulting in microhardness superior to the base metal and its stable microstructure free of thermal stresses.

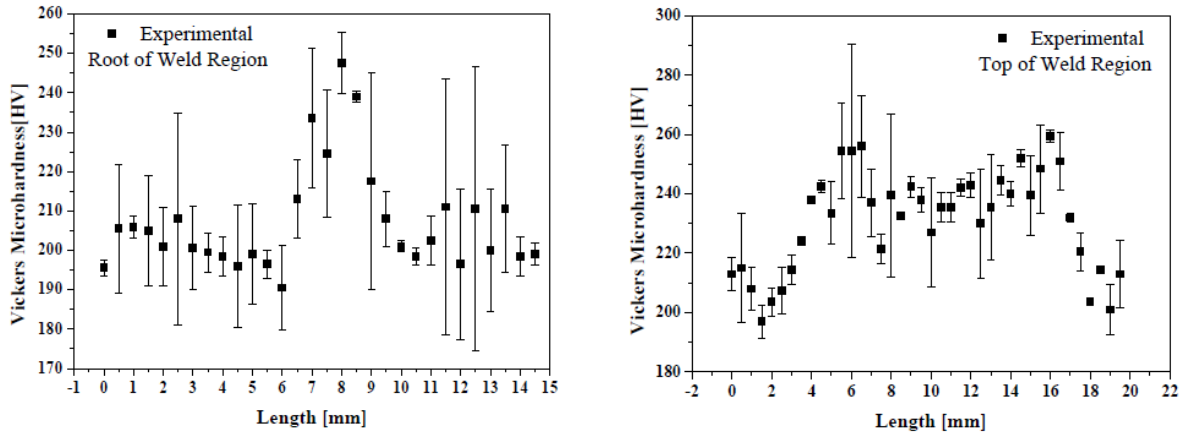

(a) (b)

Figure 11: Vickers microhardness of the studied specimen: (a) Region near the root and (b) near the upper surface.

Lower microhardness values near the weld root may also be due to stress relieving caused by subsequent passes given above the initial passes, which, by conduction transfer by the workpiece, may have rearranged the ferritic matrix and eliminated metastable carbides from sudden colds.

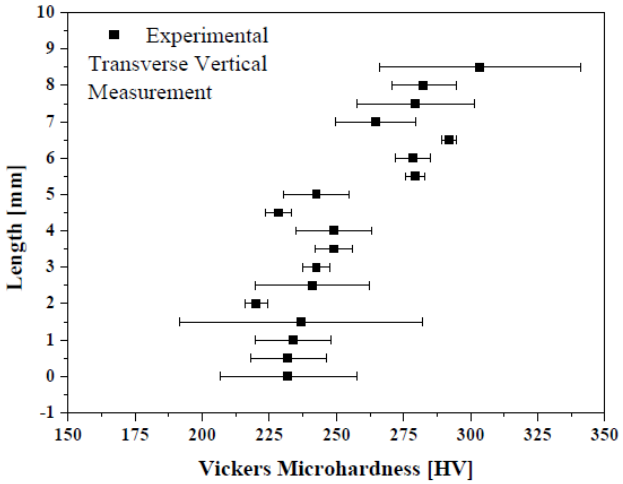

Figure 12: Vickers microhardness taken from a hypothetical vertical line from the chamfer root to the weld bead reinforcement.

4. CONCLUSIONS

After the characterization of the MAG welding process in an AISI SAE 1020 steel, it was possible to survey the following informations: welding parameters provided at the beginning of the project were not adequate, which entailed a reverse soldering. However, the optimal value is very close to the one used, since the lack of alimentation was very small; In the macrostructure, it was possible to observe the existence of epitaxial and concurrent growth, exactly as expected in multi-beam welds. It was also possible to observe that the heat-affected zone did not appear very extensive; the microstructure present in the regions closest to the top of the weld bead consists basically of hard structures and fast cooling characteristics such as Widmanstätten ferrites and martensites. In terms of microhardness, an order of 250 HV was seen in the region of the root of weld, while in the higher positions, 300 HV was collected.

5. REFERENCES

Bhatti, S., Chhabra, N. and Singh, P., 2017. "Experimental investigation of multi-pass, welding current and arc travel speed on aisi 1020 on weld joint mechanical properties during gmaw". *International Research Journal of Engineering and Technology*, pp. 2024–2029.

Chen, C., Lin, S., Fan, C., Yang, C. and Zhou, L., 2018. "Feasibility analysis of pulsed ultrasonic for controlling the gmaw process and weld appearance". *The International Journal of Advanced Manufacturing Technology*, Vol. 97, No. 9-12, pp. 3619–3624.

Della Rovere, C.A., Ribeiro, C.R., da Silva, R., de Alcântara, N.G. and Kuri, S.E., 2014. "Microestrutura e resistência à corrosão de aços inoxidáveis supermartensíticos soldados por fricção radial".

Easterling, K., 2013. *Introduction to the physical metallurgy of welding*. Elsevier.

Hackenhaar, W., Gonzalez, A.R., Machado, I.G. and Mazzaferro, J.A., 2018. "Welding parameters effect in gmaw fusion efficiency evaluation". *The International Journal of Advanced Manufacturing Technology*, Vol. 94, No. 1-4, pp. 497–507.

Lyman, T., 1972. *Metals Handbook: Atlas of Microstructures of Industrial Alloys*, Vol. 7. ASM Metals Park.

Modenesi, P.J., Marques, P.V. and Bracarense, A.Q., 2005. *Soldagem: Fundamentos e Tecnologia*. Editora UFMG.

Moyses, E.R.D.A., Mendes, T.A., Bailoni, D. and Scotti, A., 2018. "Efficacy assessment of wire cleaning and lubrification on mig/mag feedability". *Soldagem & Inspeção*, Vol. 23, No. 1, pp. 83–92.

Nunes, E.B., Batista, H.J., Barreto, A.S., Marques, J.d.S. and Motta, M.F., 2012. "Influence of the heat input on the microstructure and microhardness of weld overlay of duplex stainless steel". *Soldagem & Inspeção*, Vol. 17, No. 2, pp. 114–122.

Oliveira, G.L.d., 2013. "Soldagem dissimilar dos aços aisi 8630m e astm a182 f22 para aplicações subaquáticas". *Fortaleza: Universidade Federal do Ceará*.

Sartori, F., Silva, R.H.G., Dutra, J.C., Paes, L.E.d.S., Schwedersky, M.B. and Marques, C., 2017. "A comparative analysis of different versions of the mig/mag process modern variants for the root pass in orbital welding". *Soldagem & Inspeção*, Vol. 22, No. 4, pp. 442–452.

Sumesh, A., Nair, B.B., Rameshkumar, K., Santhakumari, A., Raja, A. and Mohandas, K., 2018. "Decision tree based weld defect classification using current and voltage signatures in gmaw process". *Materials Today: Proceedings*,

Vol. 5, No. 2, pp. 8354–8363.
Wainer, E., Brandi, S. and De Mello, F., 2004. *Soldagem: Processos e Metalurgia*. Edgar Blucher Ltda.

6. RESPONSIBILITY NOTICE

The authors are the only responsible for the printed material included in this paper.